COLLAPSE OF THE ARECIBO OBSERVATORY IN PUERTO RICO: REFLECTIONS FROM A STRUCTURAL ENGINEERING PERSPECTIVE[1]

Juan C. Morales[2] and Luis E. Suárez[3]

ABSTRACT: The suspended platform of the Arecibo Observatory collapsed on December 1, 2020, after 57 years of illustrious service to the scientific community. This article reflects on the collapse from a structural engineering perspective. It explores issues that most likely contributed, including the cable terminations and their performance under loading, corrosion, fatigue, safety factors, the dynamic demands on the remaining cables when one of them suddenly snaps, and the dynamics of the suspended platform during its pendular swing. The article is based on publicly available reports from the news media, photographs, and published video recordings of the collapse sequence. These were expanded with relevant studies collected from the literature and with publicly available technical reports from structural engineering consultants that evaluated the structure during its final months. It is organized as a sequence of events, starting with the first cable failure on August 10, 2020, the second failure on November 6, 2020, and the final collapse. Despite the limitations, it is concluded that corrosion does not seem to have played a significant role, and that the failure of the first cable was most likely due to flaws during the fabrication of the cable/socket connection. These will be reviewed and updated once the forensic analyses of the failed elements are concluded and made public.

Keywords: Arecibo Observatory, collapse, fatigue, corrosion, socket

COLAPSO DEL OBSERVATORIO DE ARECIBO EN PUERTO RICO: REFLEXIONES DESDE UNA PERSPECTIVA DE INGENIERÍA ESTRUCTURAL

RESUMEN: La plataforma suspendida del Observatorio de Arecibo colapsó el 1 de diciembre de 2020, luego de 57 años de ilustre servicio a la comunidad científica. Este artículo reflexiona sobre el colapso desde una perspectiva de ingeniería estructural. Explora los problemas que probablemente contribuyeron, incluyendo las terminaciones de los cables y su rendimiento bajo carga, la corrosión, la fatiga, los factores de seguridad, las demandas dinámicas de los cables restantes cuando uno de ellos se rompe repentinamente, y la dinámica pendular de la plataforma suspendida durante el colapso final. El artículo se basa en informes disponibles públicamente de los medios de comunicación, fotografías, y grabaciones públicas de video de la secuencia del colapso. Estos se ampliaron con estudios relevantes recopilados de la literatura y con informes técnicos disponibles públicamente de consultores de ingeniería estructural que evaluaron la estructura durante sus últimos meses. Está organizado como una secuencia de eventos, comenzando con la primera falla del cable el 10 de agosto de 2020, la segunda falla el 6 de noviembre de 2020, y el colapso final. A pesar de las limitaciones, se concluye que la corrosión no parece haber jugado un papel significativo, y que la falla del primer cable probablemente se debió a fallas durante la fabricación de la conexión del cable con su terminación. Éstos serán revisados y actualizados cuando se concluyan y se hagan públicos los análisis forenses de los elementos fallidos.

Palabras clave: Observatorio de Arecibo, colapso, fatiga, corrosión, terminación

INTRODUCTION

The suspended platform of the iconic Arecibo Observatory collapsed catastrophically on December 1, 2020, shortly before 8:00 am (Drake, 2020). The observatory, also known as the National Astronomy and Ionosphere Center (NAIC), generated a long list of illustrious scientific accomplishments since it was inaugurated on November 1, 1963, most notably the 1993 Nobel Prize in Physics that was awarded to Russell Hulse and Joseph Taylor. Their radio

[1]Article received on December 22, 2020 and accepted for publication on December 27, 2020.
[2]Professor and Head of Mechanical Engineering, Ana G. Méndez University, Gurabo Campus, PO Box 3030, Gurabo, Puerto Rico 00778. Email: jcmorales@uagm.edu
[3]Professor, Civil Engineering and Surveying Department, University of Puerto Rico-Mayaguez (UPRM), Puerto Rico 00681-9041. Email: luis.suarez3@upr.edu

astronomy work in Arecibo with a binary pulsar provided a strict test of Einstein's Theory of General Relativity and revealed the first evidence for the existence of gravitational waves (NAIC, 2020a).

The objective of this article is to reflect on the collapse from a structural engineering perspective. It explores issues that most likely contributed, including the cable terminations, corrosion, fatigue, safety factors, the dynamic response of the cables when one of them suddenly snaps, and the dynamics of the suspended platform during its pendular swing. It is based on limited information, mainly photographs, videos, and reports from the news media. These were expanded with relevant information collected from the literature and publicly available reports from structural engineering consultants of the Arecibo Observatory.

The authors are familiar with the structure. The second author served as the advisor of the first author on his PhD dissertation that investigated the dynamic properties and seismic response of the Arecibo Observatory using modern computational techniques (Morales, 2006).

The article begins with a brief background that identifies the main components of the structure. Then it sequentially addresses the failure of the first cable on August 10, 2020, the failure of the second cable on November 6, 2020, and the final collapse on December 10, 2020. Relevant information is introduced within each of these three events. The article ends with a conclusions section. The conclusions will be reviewed and updated in the near future, once the forensic analyses are completed and made public.

BACKGROUND OF THE STRUCTURE

The selected site for the observatory was a sinkhole in the mountains of Arecibo, Puerto Rico, where the limestone had collapsed almost perfectly to accommodate the 1000 ft-diameter primary reflector. Three towers were erected around the perimeter of the sinkhole and were numbered based on their position around an imaginary clock – 4, 8 and 12 – with tower 12 on the North (Figure 1(a)). The triangular platform was hoisted approximately 500 ft and suspended with cables extending from the towers. Finally, the spherical primary reflector was assembled in the sinkhole. The platform housed the electronic instrumentation that emitted and received radio waves that bounced off the 1000 ft-diameter dish. A suspended catwalk bridge and waveguide (Figure 1(b)), located near tower 12 and the control room, provided access to the platform for personnel and a path for power and instrumentation cables (NAIC, 2020b; NAIC, 2020c).

The three towers reached the same height; however, tower 8 was 120 feet taller because it was founded at the foot of a hill (Figure 1(c)). The towers had a cruciform cross section which gave them two equally strong axes, one of them aligned with the cables. The cross-sectional dimensions changed approximately every 60 feet in height as the towers were stepped in by approximately 3 feet on all sides while the thickness remained constant at 6 feet.

The 900-ton platform was suspended by 18 cables (6 per tower) whose tension was counteracted by 21 backstay cables (7 per tower). Four main cables (3.0-inch diameter) extended from a saddle on each tower to a corner of the platform. The main cables and the saddle dated from 1963. In addition, two auxiliary cables (3.25-inch diameter) extended from a collar on each tower to the 2/3 points on the sides of the platform. The auxiliary cables and collar, which dated from 1996, assisted in supporting the weight added during the Gregorian Dome upgrade and provided lateral support. Figures 1(b) and 1(d) show the arrangement of the main and auxiliary cables. Also, there was one service cable extending from each tower that connected near (not attached to) the platform and provided a support for the upper end of the catwalk bridge. The service cable is identified as "SC" in Figure 1(b). Figure 1(b) also shows the tuned mass dampers on the cables used to reduce vibrations that cause fatigue loading. Figure 3(a) shows the saddle and collar that anchor the cables on tower 4.

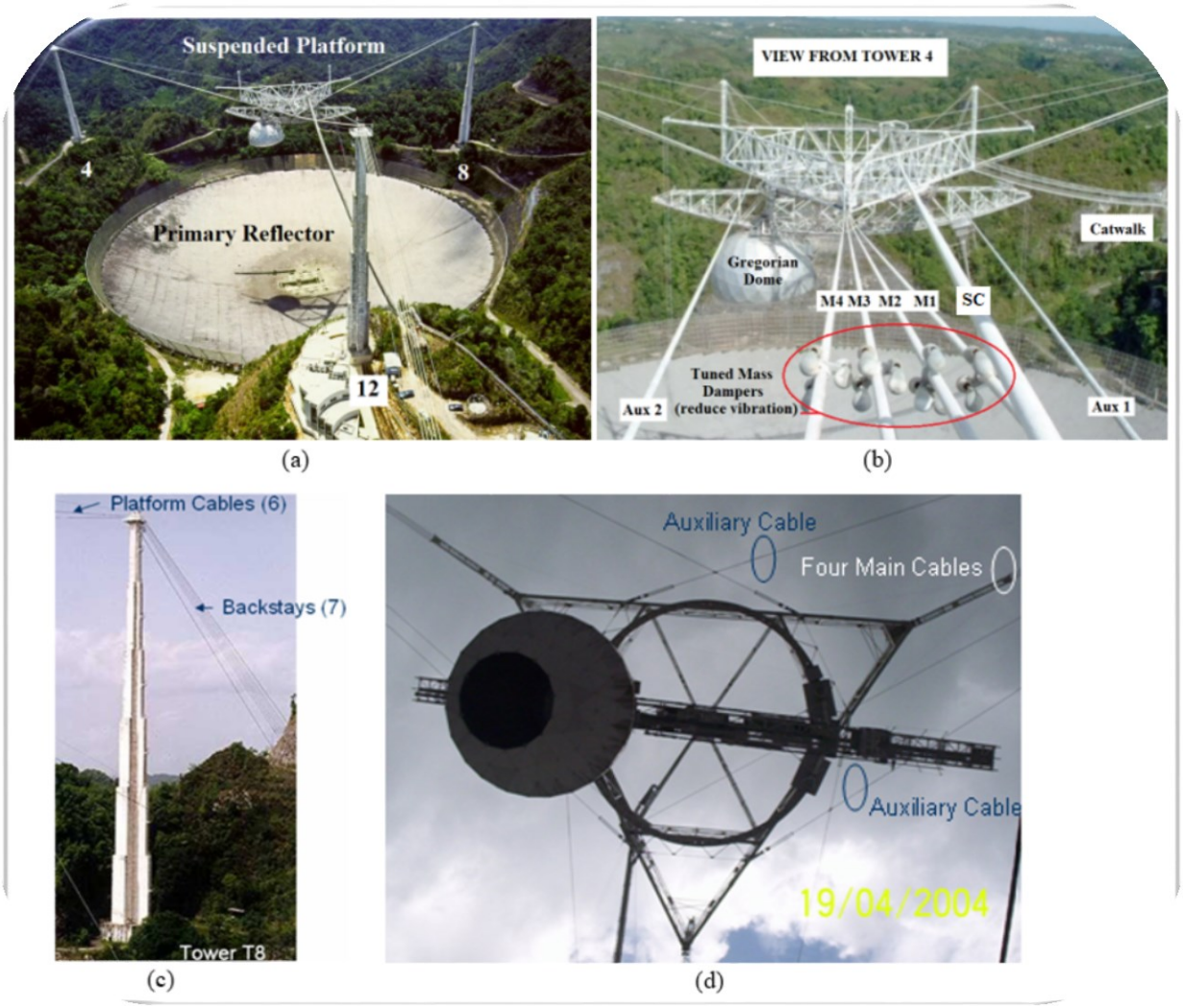

Figure 1: Several views of the structure that identify its main components. Taken from Morales (2006) except (b) which was taken from https://ecommons.cornell.edu/handle/1813/33229.

FAILURE OF THE FIRST CABLE ON AUGUST 10, 2020

The first press release from the Arecibo Observatory (NAIC, 2020d) reported that one of the auxiliary cables of Tower 4 broke on August 10 at 2:45 am. A later press release (NAIC, 2020e) reported that the break was caused by the auxiliary cable slipping out from its socket (anchorage) at tower 4. The structural engineering of record confirmed it: "…the cable pulled from its socket and fell…" (Thornton Tomasetti, 2020). The cable is identified as "Aux 1" in Figure 1(b).

This section explores the corrosion state of the failed cable, the typical process to fabricate a cable/socket connection, the performance and capacity of sockets under loading, potential fatigue zones to be examined, and the dynamic consequences of the sudden failure on the remaining cables.

Corrosion

Figure 2(a) shows a photograph of the 3.25-inch diameter cable as it lay on the dish after the failure. It shows that the cable was fabricated by wrapping a large number of small-diameter galvanized wires in a single strand to the

desired cable diameter. The wires appear in very good condition in terms of corrosion. There are some regions of whitish corrosion products of the protective zinc coat that seem to classify between Stages 1 and 2 of the Hopwood and Havens classification system for corrosion of galvanized wire, shown in Figure 2(b). There are no brownish discoloration zones that would indicate corrosion of the steel inside the zinc coat. These would have classified as Stage 3 or 4 of corrosion of the wires, but none are detected from the photograph.

Figure 2(a) also shows the cylindrical-shaped end of the cable near the top of the photograph. The length of the cylindrical end is approximately three times the cable diameter. It seems mostly intact and free of corrosion. The wires on the end appear to have been unwound and separated during the brooming process (addressed in the next section). Based on its cylindrical shape, the cable clearly appears to have failed by slipping out of its socket anchorage, as reported. However, there are also several unattached wires surrounding the broomed end which will be addressed later.

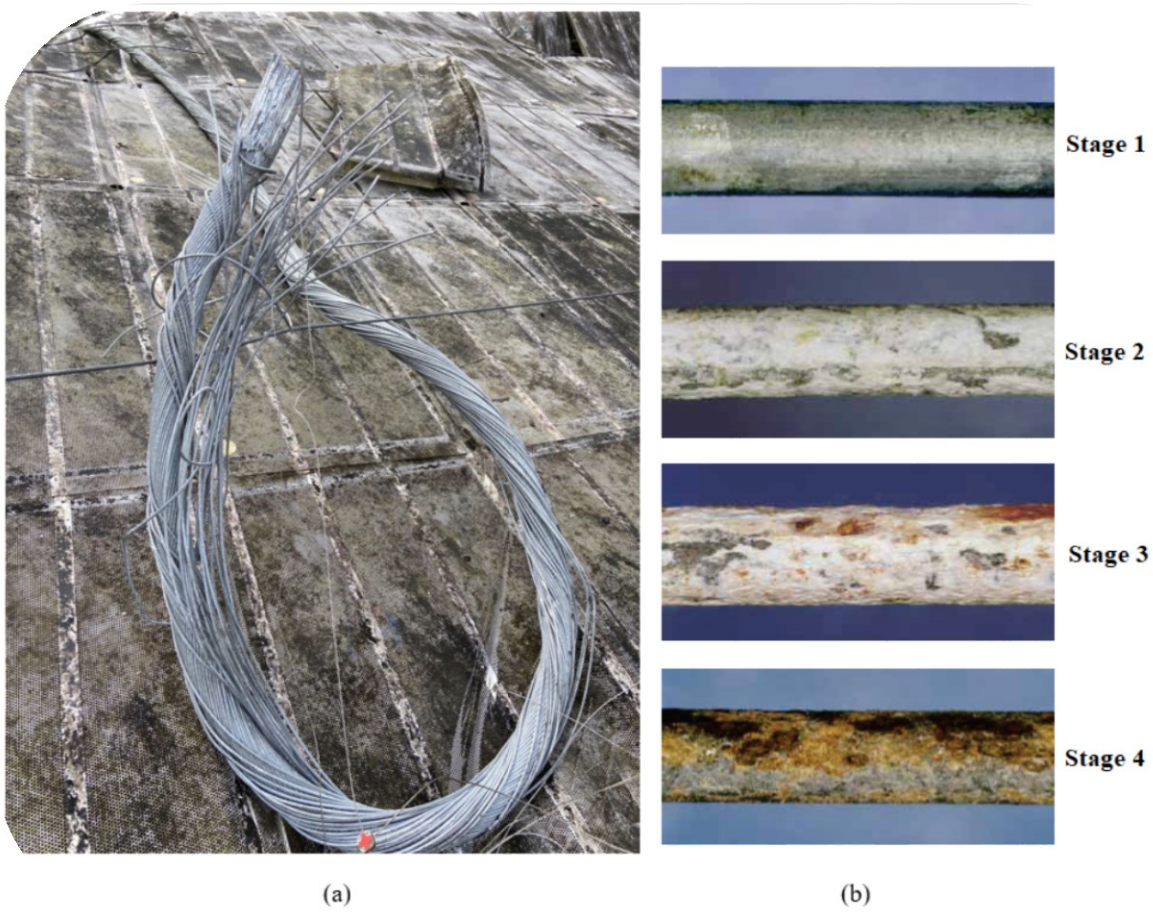

Figure 2: (a) Photograph of the auxiliary cable after failure. Taken from Wall (2020). (b) Photographs of the four stages of galvanized wire corrosion based on the Hopwood and Havens classification system. Taken from Chavel and Leshko (2012).

Identification of socket

Figure 3(a) shows a photograph of the top of tower 4 at the instant that the remaining three main cables failed. It shows the socket of the remaining auxiliary cable below the word "Drone" and includes approximate dimensions that were scaled off using the 3.25-inch diameter cable as the basis. It was presumably identical to the socket involved in the failure; whose anchor hole is seen on the left of the photo. The failed socket had been removed and lowered for forensic analysis. The auxiliary cable entered the socket at the lower-left end, the load was transferred to the socket

in the ~12 in conical section, and the clevis joint transferred the load to the collar. Slippage occurred from the ~12-inch conical section of the socket. Figure 3(b) shows that typical sockets are also conical on the inside and this internal conical volume is called the "basket" of the socket.

The federal specification RR-S-550 Rev. D (1980) specifies a basket whose length is 3.7 times the cable diameter, for the case of the largest diameter cable that they specify (2.625 inch). The updated specification (RR-S-550 Rev. F, 2018) still specifies the same ratio of basket length to cable diameter. If the 3.7 ratio was maintained for the 3.25-inch diameter auxiliary cable, then the basket length would be calculated at 12 inches which agrees with the scaled-off dimension shown in Figure 3(a).

Judging from Figure 2(a), the end of the cable that went into the socket appears to be only 3.0 times the cable diameter, i.e., it appears to be shorter than the basket size of the socket.

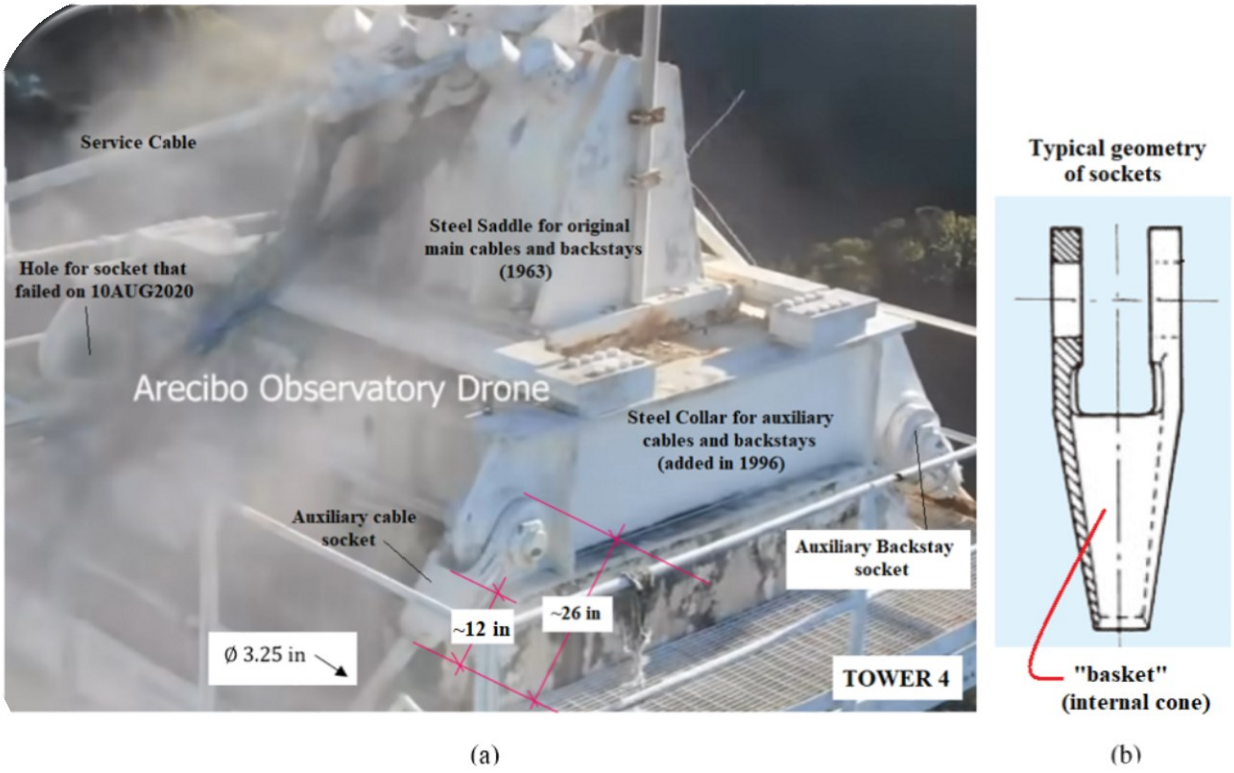

Figure 3: (a) Photograph of the top of tower 4 during final collapse. Taken from the NSF video (2020a). It shows the location of the sockets and their approximate dimensions (scaled off). (b) Typical geometry of a socket that shows its internal conical shaped basket. Taken from Tokyo (2020).

Process to fabricate the cable/socket bond

Manufacturing flaws in the process of bonding the cable to the socket may have played a part in the pull-out failure. The details of the Arecibo sockets, and the manufacturing process used to bond them to the cables, are unknown to the authors. To the best of the authors knowledge, the spelter (molten metal) used to bond the Arecibo sockets was molten zinc.

Certex (2020, p. 4-11) provides a series of steps for zinc spelter sockets that are summarized below. The steps should be similar to the process used for the Arecibo sockets, and they are included to provide a basis to reflect on potential issues.

1. Measure the length of cable that will be inserted in the socket and seize it with wire at that location (to avoid unwinding the wires below the socket), in preparation for brooming.

2. Prepare the broom at the end of the cable, i.e., unwind and separate the wires all the way down to the seizing. (Figure 4(a)). The brooming procedure increases the surface area available for bonding because each wire participates in transferring load to the socket. The greater the surface area for bonding, the greater the resistance. For example, for a hypothetical 3.25-inch diameter cable fabricated from 76 individual wires with an average diameter of 0.274-inch, the bonding surface area increases by a factor of 6.4 when each individual wire is bonded versus simply bonding the outside diameter of the 3.25-inch cable.

3. Thoroughly degrease, clean, and dry the individual wire strands in the broom.

4. Orient the cable vertically, place it in a vise, and close the broom with seizing cable. Once opened, the broom must be closed temporarily so that it can fit through the hole in the socket. Ensure a "minimum vertical length of rope extending from the socket equal to about 30 cable diameters. This vertical length is necessary for cable balance. Premature wire breaks at the socket can occur if the cable is not balanced at pouring".

5. Heat the socket to the appropriate temperature and insert the cable in the socket basket (internal cone). The socket is heated to prevent the molten zinc from cooling and solidifying too quickly when the zinc is eventually poured into the basket. The molten zinc must reach the bottom of the basket. "A word of caution: Never heat a socket after it is placed on a cable. To do so may cause damage to the cable".

6. Untie the broom and separate the wires into the cone shape inside the basket. The wires must extend to the top of the basket (Figure 4(b)). "Use extreme care in aligning the socket with the cable's centerline".

7. Pour the molten zinc (spelter) into the socket basket (Figure 4(c)) at a temperature of 950-1000 degrees F. "A word of caution: Overheating of the zinc may affect its bonding properties". "Pour the zinc in one continuous stream until it reaches the top of the basket and all wire ends are covered". Allow the zinc to cool.

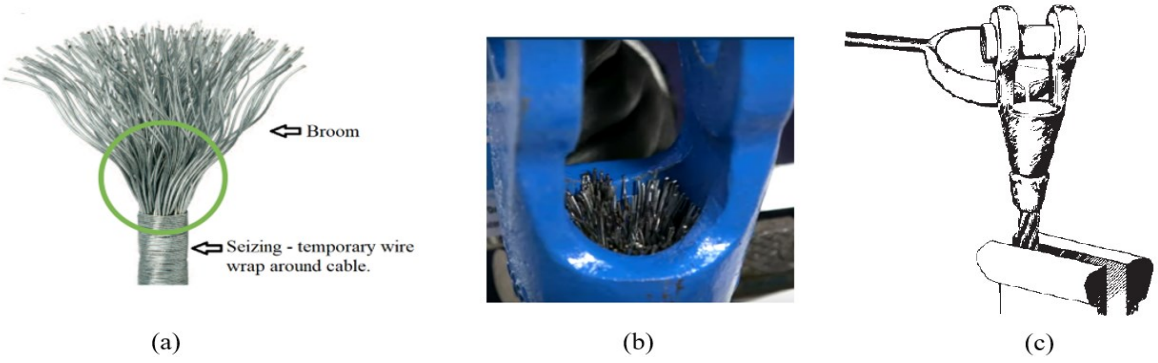

Figure 4: (a) Broom at the end of the cable and the "seizing" (taken from Wirelock, 2017). (b) Socket after inserting the cable and re-separating the broom wires (taken from Wirelock, 2017). (c) Pouring the molten zinc into the socket (taken from Certex, 2020).

Discussion of manufacturing challenges during the bonding of the cable to the socket

The manufacturing process summarized above points at several potential challenges. One of them is size. The Arecibo cable weighed approximately 30 lb/ft and the socket weighed another 200-300 lb. which would require mechanical equipment to handle it, even for the cleaning operations (step 3) which require good workmanship.

Size also comes into play while setting up for the zinc pour. A vertical length of 30 cable diameters below the socket is recommended (step 4). For a 3.25-inch diameter cable, a minimum of 8 feet would be required. If four additional feet are added to provide a radius for the cable as it nears the floor, plus 3 feet for the overall length of the socket, the process had to be conducted at approximately 15 feet above the floor of the shop.

The socket had to be heated before sliding it into the cable. Additional heat input is not allowed after the cable is inserted because it could damage the cable (step 6). Size comes into play once again. The socket had to be handled relatively quickly during the cable insertion to avoid unfavorable cooling. Then, the temporary seizing on the cable had to be removed, and the wires spread out once again into a cone shaped broom, while working within the hot socket. There seems to be good potential at this point for poor workmanship. If the re-formation of the broom ended up more cylindrical than conical in shape, slippage would be induced.

The zinc pour also presents a challenge. If the zinc were overheated, it could have affected its bonding properties (step 7). Size also comes into play because the Arecibo socket had a ~12-inch-long basket that required a substantial volume of molten zinc. Step 7 requires a continuous pour from start to finish.

This was not a trivial process. It would have required good planning, a good setup to work at a height of approximately 15 feet above the floor shop, and trials to ensure that the entire process could be conducted appropriately within a specified amount of time to avoid undue cooling of the socket and the molten zinc prior to the pour.

Literature review of socket performance under loading

Bradon and Ridge (2003) conducted single-wire pull-out laboratory tests for a molten lead-alloy spelter (Arecibo's spelter was presumably molten zinc and would exhibit similar performance). The objective was to determine if the bonding between the wires and the spelter could be sufficient to hold the wire. They considered various lengths of embedment on a cylindrical (not conical) test piece. The results showed a high degree of scatter; however, in the case of an embedded length of 5.4 times the diameter of the cable, the wire broke before slipping in three out of the four tests that they conducted. They attributed the scatter to three possibilities: incomplete wetting of the entire wire; breakdown of the bond where the wire entered the spelter due to shrinking of the spelter upon cooling; and/or traces of contaminants that prevented full bonding from taking place. Due to the high scatter in the data, they concluded that bonding on its own, although significant, is not sufficiently reliable.

In addition, they reported that the load is also transferred by the frictional force developed between the wire and the spelter due to the conical spelter's wedging action against the confinement provided by the conical socket. They instrumented the outside of the sockets with strain gauges and determined that the load was transferred throughout the entire length of the socket for metal poured sockets. In one of the samples – sample 3 – there was incomplete wetting (bonding) at the entrance to the socket. It resulted in low strain gauge readings at the entry point but higher load transfer at the opposite end, i.e., it compensated. They also found that upon removal of the load, the hoop (circumferential) strains in the socket dropped only slightly, suggesting that "an irreversible 'wedging' action was taking place, with the spelter cone moving relative to the socket under load and remaining wedged in this position even when the load was removed". They attempted to measure the movement (draw) of the spelter cone when loaded; however, their method proved unsuccessful due to "the very small draw values observed in the tests". As a final note, they only increased the load to approximately 70% of the cable breaking strength since the objective was to investigate the mechanism of load transfer.

On the other hand, Metcalf and Matanzo (1980) conducted tests up to failure. They wanted to determine the performance of nine of the best-known cable terminations under static and fatigue loading, including a zinc poured socket similar to the one at Arecibo. They fabricated several specimens of each of the nine types under controlled

shop conditions and included flawed specimens to evaluate the effect of poor workmanship on the strength of the cable termination. In the case of the zinc poured socket assembly, they investigated poor workmanship due to the elimination of the acid wash of the broomed end.

On the pull test (static load) of a 2-inch diameter cable, the zinc poured socket achieved the highest efficiency among the nine terminations. Efficiency was defined as the specimen breaking load divided by the maximum breaking load. A 98% efficiency was achieved with the zinc poured socket (from Table 1 in the article). The failure modes observed for the static test were given in Table 7 of the article and are included here:

- 55% - Multiple strand breaks inside or at base of socket
- 40% - Multiple strand breaks in gage area (away from the socket)
- 5% - Rope pulled out of socket (This was the second-lowest percentage of pull-outs of all nine terminations, with the lowest at 4% and the highest at 9%)

Service life tests (fatigue loading) were conducted on a vertical fatigue testing machine which, for the 2-inch diameter cable, applied an oscillating load at a frequency of 12 Hz that ranged over 25% of the Catalog Breaking Strength (CBS) of the cable. The cyclic load was superimposed over a mean stress of 17.5% of the CBS. "For the fatigue tests, failure was defined as twenty broken wires at the base of the termination fitting, or one million cycles, whichever came first". The zinc poured socket's efficiency was 99%, including the flawed specimens (from Table 2 in the article). The failure modes observed for the fatigue tests were given in Table 8 of the article and are included here:

- 100% - Multiple strand breaks inside or at base of socket

In Table 6 they recommended frequent inspections to search for broken wires at the base of the zinc poured socket. They add: "It is imperative that an inspector have a clear-cut set of instructions to guide him in determining exactly when a particular wire rope termination must be taken out of service. The replacement criterion proposed is that replacement be required if the inspector detects cracks in the pressed sleeve or socket body, or ten (10) broken wires in the adjoining wire rope."

Detached wires around end of failed cable: a fatigue issue?

Figure 5(a) zooms in on the broomed end shown in Figure 2(a) and shows approximately 20 detached wires surrounding the broomed end (circled in yellow). Metcalf and Matanzo (1980) observed that 100% of the wire fatigue failures were located either inside or at the base of the socket. These detached wires would therefore be at the predicted location for fatigue failures. If fatigue were the cause, the wire breaks would have taken place before the failure on August 10, 2020 and would have been identifiable. It is unknown to the authors if wire breaks were present before failure. Thornton Tomasetti (2020) mentions "a few documented wire breaks on the original cables over the years".

Another possible mechanism for these detached wires is that they became unbonded or that they broke off due to the impact of the fall from the tower (~500 ft). A forensic inspection of the fracture zones of the cables (the tips) with a Scanning Electron Microscope (SEM) would most probably be able to detect fatigue signatures such as crack initiation sites and "beach marks".

Another interesting area to conduct a forensic inspection with a SEM is the circled zone in Figure 5(b) which zooms in at the bottom of the broomed end. Wire breaks appear to have occurred in this zone, either by fatigue, or by the impact of the fall.

Nevertheless, if fatigue had been the primary failure mechanism, then the cable should have failed, not by slipping from the socket, but by rupturing near the base of the socket. The fact that the broomed end seems almost intact (Figure 5(a)), points at slippage from the socket as the cause of failure, even if all of the 20 wires circled in yellow had failed by fatigue. Also, Metcalf and Matanzo (1980) observed that pull-out failures occurred only in cases of static loading. Therefore, it appears that the slip mechanism is mostly associated to the capacity of the socket assembly for static load resistance rather than a fatigue-cycling condition.

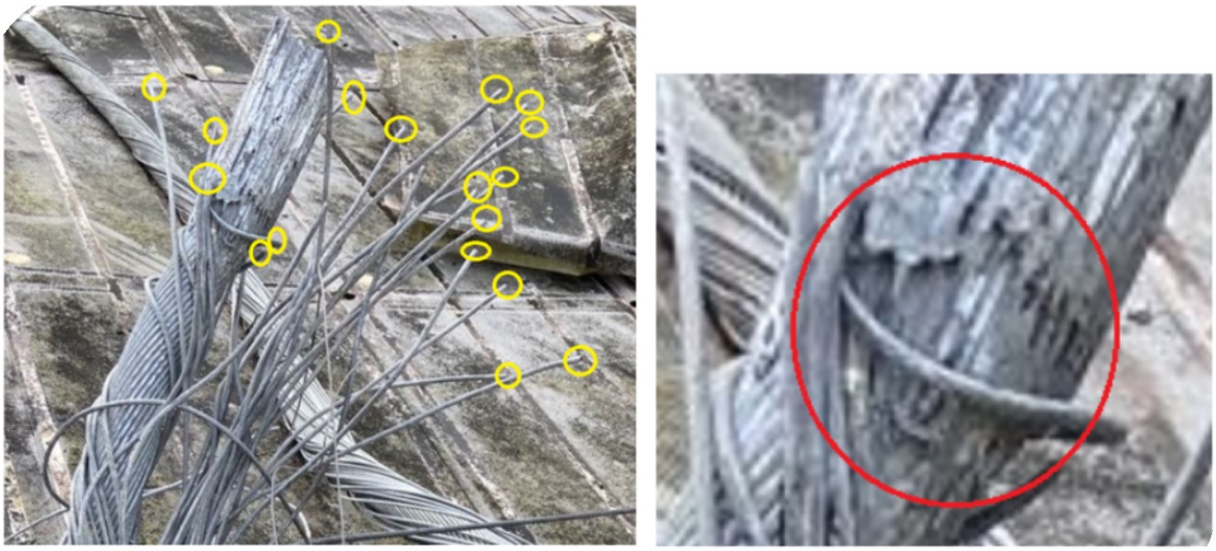

Figure 5. (a) Detail of the broomed end showing detached tables (yellow circles) that could have failed either by fatigue or by detachment/breakage due to the impact of the ~500 ft fall. (b) Detail of the bottom of the broomed end showing a potential zone where cables broke off (red circle). Taken from Wall (2020).

Is further research required on the length of the spelter cone?

The Bradon and Ridge (2003) single-wire pull-out results showed that when the embedment length was 5.4 times the cable diameter, in 3 out of the 4 tests the wires broke instead of pulling out. As mentioned earlier, the basket length in the Arecibo socket was approximately 3.7 times the cable diameter. This satisfied the federal specification RR-S-550 Rev. D (1980) and its more recent Revision F of 2018 which also showed a ratio of 3.7 for the largest sized cable that they address (2.625-inch diameter).

However, the German standard DIN 3092-1 (1985) specifies a minimum spelter cone length 5.0 times the cable diameter for wire ropes ("wire rope" is a type of steel cable fabricated similarly but not equally to the Arecibo cables: wires are first wound into intermediate-sized strands which are then wound to the final diameter of the wire rope. The Arecibo cables were wound into a single strand and is known as "strand" cable instead of "wire rope".).

Citing from Verreet (1997): "In accordance with DIN 3092, the opening angle of a wire rope socket should be between 5˚ and 18˚, and the length of the spelter cone should be at least five times the nominal rope diameter. Break tests have proved that, even with shorter spelter cone lengths, the full breaking strength of the rope can be transferred". They note that shorter lengths have worked but the standard still specifies the minimum of 5.0 times the diameter of the cable.

A 5.0 minimum ratio between the cone length and the cable diameter would add reliability to the socket. It would be very comforting to assume that a cable failure should take place in the cable itself by rupturing rather than by slippage from the termination. It may be asked, is more research required on these types of terminations to increase the level of reliability? The research would need to consider the manufacturing implications because it would increase the required level of workmanship to properly manufacture it. As noted previously, it is already challenging to manufacture it at a 3.7 ratio.

The cable that failed was apparently not the only one with slippage problems. Citing from Thornton Tomasetti (2020), "Furthermore, TT recommended the replacement of all of the auxiliary cables, since the one 3¼-inch auxiliary cable completely pulled from its socket and numerous other auxiliary cables exhibited unusual slip at their sockets". In the case of the socket shown in Figure 3(a), the photograph shows that the remaining auxiliary cable did not appear to be one of the cables with slippage problems.

Dynamic consequences of a cable failure on the remaining cables

This section investigates the dynamic effects on the remaining cables of a multi-cable structure caused by the sudden loss of a single cable. It derives a *dynamic amplification coefficient* α assuming a single degree of freedom system. In the case of the Arecibo Observatory, assuming that the damping ratio of the cables was $\xi = 0.05$, the dynamic amplification coefficient is calculated at $\alpha = 1.85$. This means that the load added by the sudden failure of the cable was momentarily increased by 85% over its static value. In addition, a *dynamic redistribution coefficient* β is also derived to distribute the dynamically amplified load into all the remaining cables. The factor β is a function of the number of cables and the previous coefficient α.

In the case of Arecibo, two cases were considered to bound the results. The first case (lower bound) assumes that all the cables participate, and so $N = 18$ cables. In that case, $\beta = 1.05$. The second case assumes that only the cables in one tower participate and therefore $N = 6$. This second case provides an upper bound and seems appropriate given the uncertainties with the amount of damping offered by the platform and its 3D rotational degrees of freedom. For $N = 6$, the calculations result in $\beta = 1.14$. This means that the instantaneous dynamic force in the remaining cables of Tower 4 would have momentarily increased by between 5% - 14% over its static value. The analytical model was verified against a 2D, multi-degree of freedom model in the program SAP2000 and the error was less than 3%, which validates the analytical model. The derivation of the two coefficients α and β are provided next.

Consider a simple model of a planar structure consisting of a weight W supported by N cables or springs. All the cables are assumed to have the same stiffness coefficient. Each cable supports a static force with amplitude $F_{cable} = W/N$. If one of the cables (springs) is suddenly removed, the structure will vibrate. This phenomenon may be confused with an initial displacement type of problem, but it is actually a forced vibration condition. Suppose that one cable is slowly removed. Its force will be distributed among the remaining N-1 cables. Evidently, the total new force acting on each of the N-1 cables is $F_{new} = W/(N\text{-}1)$. It is convenient to obtain an expression for the additional force F_{add} caused by the loss of one support, as follows:

$$F_{new} = \frac{W}{N} + F_{add} = \frac{W}{N-1} \quad \Rightarrow \quad F_{add} = \frac{W}{N\left(N-1\right)} \tag{1}$$

However, if one of the cables is suddenly removed, the force F_{add} is not slowly added to the original load W/N, but rather its time variation has the shape of a unit step function $U(t)$ (sometimes referred to as the Heaviside function):

$$F(t) = F_{add}\, U(t) \tag{2}$$

This force is shown in Figure 6 where a value of 10 kip was arbitrarily selected for F_{add}.

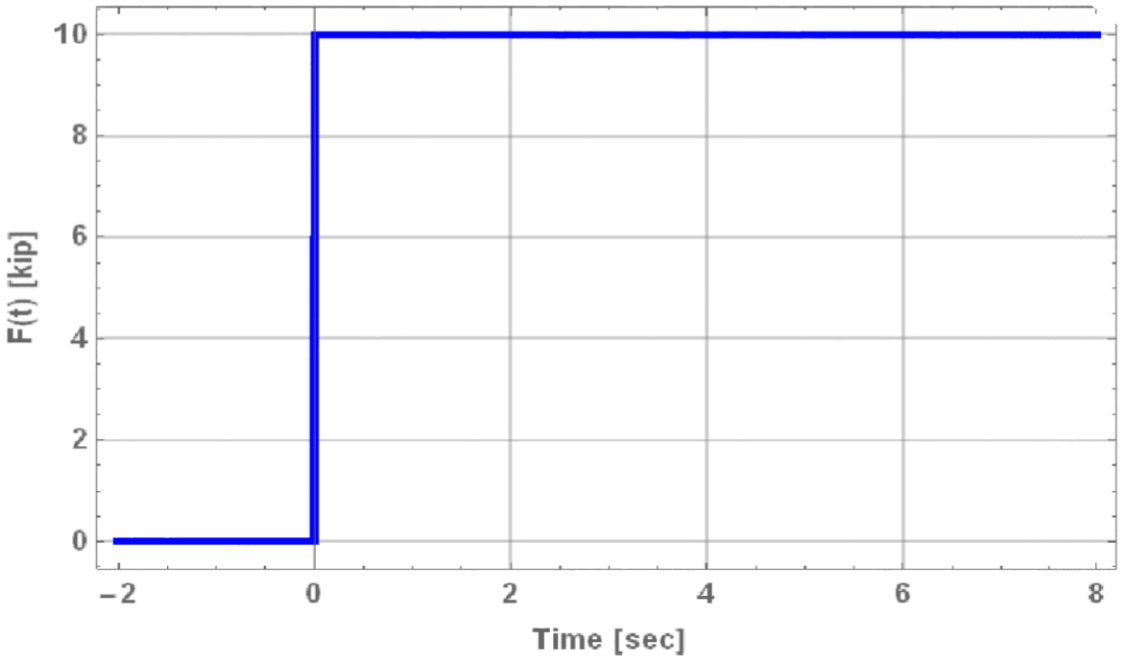

Figure 6: Step function load applied to the remaining cables.

It can be shown that when a damped single degree of freedom oscillator is subjected to a dynamic load with a step-function variation and an amplitude F_{add}, the internal force in its spring is given by:

$$F(t) = F_{add}\left[1 - e^{-\xi \omega_n t}\left(\cos(\omega_d t) + \frac{\xi}{\sqrt{1-\xi^2}}\sin(\omega_d t)\right)\right] \tag{3}$$

where ω_d is the damped natural frequency, which can be expressed in terms of the damped natural period T_d as:

$$\omega_d = \frac{2\pi}{T_d} \tag{4}$$

The damped natural frequency is in turn defined in terms of the undamped natural frequency ω_n and damping ratio ξ as:

$$T_d = \frac{2\pi}{\omega_n\sqrt{1-\xi^2}} \tag{5}$$

The force $F(t)$ attains its maximum value at a time $t = T_d/2$. Substituting this time t, as well as ω_d and T_d in equation (3) one obtains

$$F_{\max} = F_{add}\left(1 + e^{-\frac{\pi\xi}{\sqrt{1-\xi^2}}}\right) \tag{6}$$

Introducing a dynamic amplification coefficient α defined as:

$$\alpha = 1 + e^{-\frac{\pi\xi}{\sqrt{1-\xi^2}}} \tag{7}$$

The maximum force can be written as:

$$F_{\max} = \alpha F_{add} \tag{8}$$

For an undamped system (with $\xi = 0$), the maximum force F_{max} in the spring is $2xF_{add}$, i.e., twice the value as if the force $F(t)$ were applied very slowly. For other values of the damping ratio, the ratio α between the maximum dynamic and static force varies as shown in Figure 7.

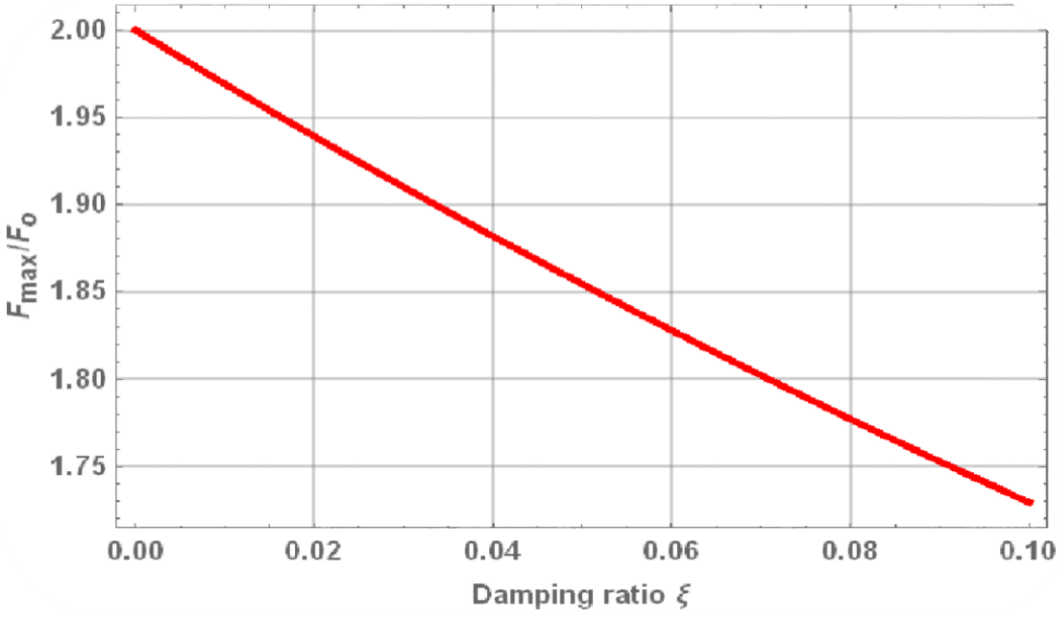

Figure 7: Variation of the ratio α between the maximum dynamic and static force as a function of the damping ratio.

Note that a damping ratio equal to 0.1 or higher is only achievable by adding external devices, such as viscous fluid dampers, treatment with damping layers, etc. For a naturally occurring energy dissipation and for a metal structure with the material below yielding, the values of ξ range from 0.005 to 0.02. For these values, the ratio $\alpha = F_{max}/F_{add}$ varies from 1.98 to 1.94. The value $\xi = 0.05$ is usually adopted when the material is at or above the yielding level.

Based on equation (1), the new force acting on the remaining cables, which now we will refer to as F_{static}, is:

$$F_{static} = \frac{W}{N-1} = \frac{W}{N} + F_{add} \qquad \text{where:} \quad F_{add} = \frac{W}{N(N-1)} \tag{9}$$

However, based on the previous demonstration, if one wants to obtain the maximum value of the force on each of the remaining cables that accounts for the dynamic effect, this new force is:

$$F_{dynamic} = \frac{W}{N} + F_{\max} \qquad \text{where:} \quad F_{\max} = \alpha \frac{W}{N(N-1)} \tag{10}$$

which can be more conveniently expressed in terms of a dynamic redistribution coefficient as:

$$F_{dynamic} = \beta F_{static} \tag{11}$$

where:

$$\beta = \frac{N + \alpha - 1}{N} \qquad ; \qquad F_{static} = \frac{W}{N-1} \tag{12}$$

We will apply now the formulas selecting first a 5% damping ratio. The dynamic amplification coefficient α is:

$$\alpha = 1 + e^{-\frac{\pi 0.05}{\sqrt{1-0.05^2}}} = 1.85 \tag{13}$$

The dynamic redistribution coefficient is now only a function of the number of cables N:

$$\beta = \frac{N + 0.8545}{N} \tag{14}$$

Figure 8 displays the variation of the dynamic distribution coefficient β that permits to calculate the maximum dynamic force by amplifying the static force as $F_{dynamic} = \beta F_{static}$:

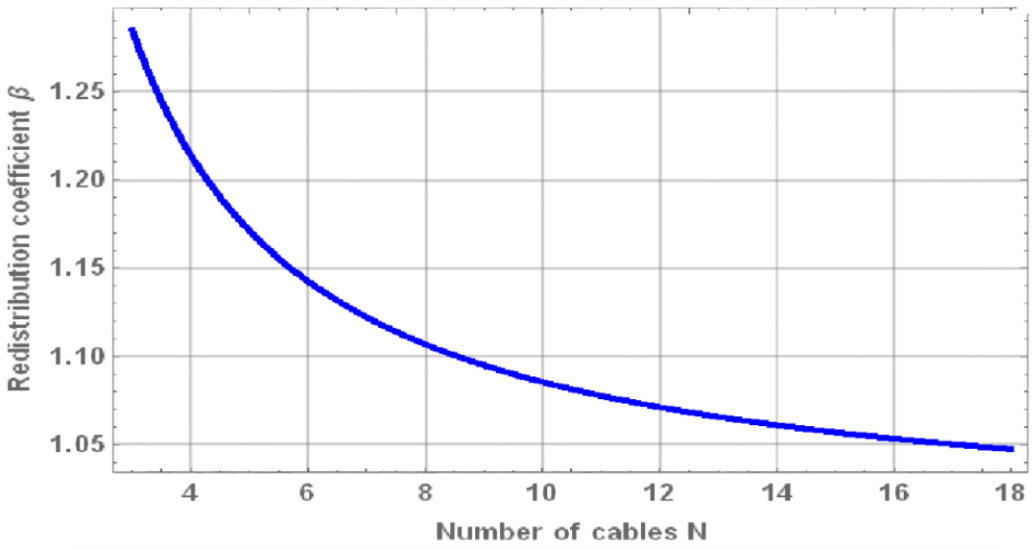

Figure 8: Variation of the dynamic redistribution coefficient β as a function of the number of cables for a 5% damping ratio.

The objective of this section was to show with simple examples that the breakage of one of the cables in a cable-supported structure introduces dynamic effects in the response of the remaining cables, which translate into a maximum instantaneous axial force larger than the one predicted by a static analysis. This situation undoubtedly occurred in the cables of the Arecibo Observatory. The dynamic effects probably increased the size of any pre-existing fatigue cracks in the remaining cables. This would have weakened the cables even further and decreased their factors of safety below the values calculated by Thornton Tomasetti (2020). These are discussed next.

State of the structure after the failure of the first cable

Thornton Tomasetti (2020) indicated that the safety factor was a suitable 1.67 on the second cable that would eventually end up failing. It was reduced from 2.1, but a factor of 1.67 still provided a suitable safety margin. The calculation was based on the reported 1,044 kip breaking strength of the cable. Citing from Thornton Tomasetti (2020), "After the failure (of the first cable), observatory staff, TT, WJE and WSP inspected/reviewed the remaining structure for signs of distress and deterioration. Given the generally good appearance of the remaining elements; suitable factor-of-safety remaining in the platform elements, as shown through analysis; and adequate redundancy of the cable system, we believed the platform to be stable then and for some time forward. Our analysis had shown that the loss of another cable would not cause catastrophic collapse of the platform. Therefore, we believed work to stabilize the structure could begin, with continuous monitoring and safe operational procedures. The observatory procured materials and supplies and planned for installation."

FAILURE OF SECOND CABLE ON NOVEMBER 6, 2020

The second cable failed 88 days after the failure of the first cable. Following this second failure, the press release of the Arecibo Observatory (NAIC, 2020e) reported the following: "A main cable that supports the Arecibo Observatory broke Friday (November 6) at 7:39 p.m. Puerto Rico time. Unlike the auxiliary cable that failed at the same facility on August 10, this main cable did not slip out of its socket. It broke and fell onto the reflector dish below, causing additional damage to the dish and other nearby cables. Both cables were connected to the same support tower (tower 4)". The cable is identified as M4 in Figure 1(b) and Figure 9.

Figure 9 shows a photograph of the original saddle of tower 4 just prior to the final collapse. The wires within a red oval are the remnants of the second cable that failed (identified as M4 in Figure 9). This was confirmed by NSF (2020b). The remnants of the cable establish that the cable ruptured, instead of slipping out from its termination. The fact that the rupture occurred near its anchorage point is consistent with the findings of Metcalf and Matanzo (1980) that 100% of the fatigue failures occur near or inside the termination. The cable ends are the most vulnerable because they are the weakened the most during fatigue loading caused by the oscillations (vibration) of the cable. Figure 1(b) shows the tuned mass dampers that were used in the main cables to mitigate the vibration effects.

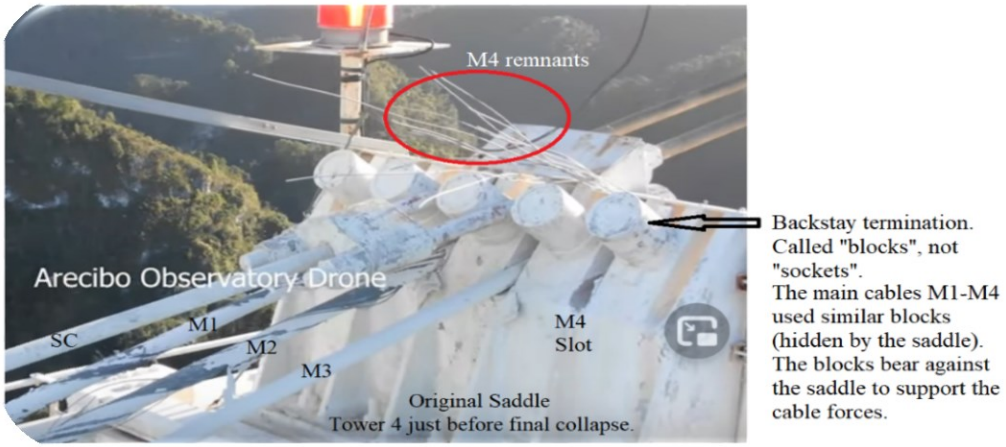

Figure 9: Photo of main saddle on Tower 4 just prior to the final collapse. The cable identifiers are consistent with Figure 1(b). Taken from NSF (2020a).

The second cable failed at a load significantly lower than its breaking strength. The calculated safety factor was 1.67 as reported previously. According to Thornton Tomasetti (2020), the "weather at the time of failure was calm, with no unusual winds or ambient temperatures and no ground shaking. Failure was unexpected". Accumulated fatigue damage throughout the 57 years of operation most likely played a role in the unexpected failure. Also, the dynamic demand of the sudden failure of the first cable would have shortened the remaining life of the cable even further, as discussed previously.

Different cable terminations: "Blocks" instead of "Sockets"

Figure 9 also shows the five cylindrical terminations of each of the five backstays. These are called "blocks" instead of "sockets". The main cables M1-M4 used similar blocks that were located on the rear of the saddle and are hidden from view in Figure 9. These blocks beared against the saddle to resist the cable forces. The details of the blocks are unknown to the authors; however, similar blocks are used in some cable stayed bridges. In these, the outside is cylindrical, but they are conical on the inside; the wires are splayed at the entrance and terminate at a locking plate; and the internal conical section is filled with a bonding agent (National Academies, 2005, p. 11). There is some similarity with the sockets of the auxiliary cables except that, instead of a clevis joint, the load is transferred by bearing against a saddle. Another significant difference is that the ends of each wire are locked in a plate. The locking plate provides an additional load transfer mechanism against slippage.

It is interesting that the blocks of the main cables dated from 1963 while the sockets of the auxiliary cables dated from 1996; yet the older termination properly anchored the main cable M4 in place. In fact, all 27 block terminations (9 per tower) held in place during the 57-year life of the structure. The authors reflect that this type of termination had the required level of reliability that would be warranted for the observatory's design, i.e., that, in case of failure, the failure should take place in the cable itself by rupturing, not by slippage from the termination.

State of the structure after the second cable failure

Citing from Thornton Tomasetti (2020), "With the loss of two cables, there are now three original cables (of four) and one auxiliary cable (of two) connecting the platform to Tower 4. Should another of these three original cables fail, the two remaining original cables will undergo static force demands at or above the specified minimum breaking strength. A catastrophic failure would be very likely. These cables are not capable of handling the required dynamic demands of a sudden failure of an adjacent cable. The structural redundancy is no longer available and cannot be factored into determining safety".

Thornton Tomasetti (2020) constructed a finite element model of the complete structure and considered several scenarios on how to reduce the load on the remaining cables (all are detailed in the reference). These included relaxation of the backstays, installation of a temporary cable, removal of counterweights from the Azimuth arm, and cutting the M4 cable that was hanging from the platform, among others.

However, the report states "We have noted wire breaks on the three remaining 3-inch-diameter original cables from Tower 4, which occurred during the November event. We continue to monitor the structure and continue to note wire breaks since the failure last week. Furthermore, there is no evidence that the existing original cables can achieve the specified minimum breaking strength and certainly evidence to the contrary, since one failed at 62% of this strength" (Thornton Tomasetti, 2020).

At this point, Thornton Tomasetti recommended decommissioning and a controlled demolition. WSP (2020) concurred with this recommendation and mentioned that "Since we are observing additional wire breaks, this leads us to believe that there is additional degradation of the cables and therefore less capacity than expected".

On the other hand, WJE (2020) proposed stabilizing the structure. As a first step, they considered proof loading the structure, i.e., adding some load to prove that it could resist it. Citing from WJE (2020), "The key element in pursuing this path is reducing structural uncertainty to acceptable levels by demonstrating that key elements have the capacities needed to support the work that must be done." Also, "Since the alternative to repair is demolition of the

facility, the risk of possibly collapsing the unoccupied structure during an attempt to save it may be acceptable." They proposed to proof load the structure by tensioning the vertical tiedown cables on the corners of the platform.

On November 19, 2020, a press release from the Arecibo Observatory announced the decision of NSF to decommission and demolish the structure (NAIC, 2020f).

FINAL COLLAPSE ON DECEMBER 1, 2020

The structure survived for 25 days after the failure of the second cable. The wire breaks mentioned by Thornton Tomasetti (2020) were also reported in the news media; for example, nine days into this period, Coto (2020) reported that "university officials say crews have already noticed wire breaks on two of the remaining main cables". Figure 9 confirms the breaks in cables M1 and M2. The breaks are easily noticed because the paint flakes off as a result of the sudden snap (NSF, 2020b). The wire breaks occurred near the termination, as predicted by Metcalf and Matanzo (1980) for fatigue loading. The paint on cables M3 and the service cable SC is still intact. In the case of the service cable, there was no overload since it only supported the catwalk bridge.

Corrosion

The loss of paint on cables M1 and M2 offers a glimpse of the cables to evaluate their corrosion state. Figure 9 shows that the cables had a grayish color which is consistent with no corrosion issues, perhaps in the Stage 1 of corrosion based on Figure 2(b). In addition, the saddle and the blocks that terminate the backstays also appear free of corrosion.

Sequence of failures during collapse

The drone video (NSF, 2020a) shows that the sequence of cable failures took place in approximately 1 second. Cable M2 was the first to break, followed by M1, and finally M3. The order of failure is consistent with observations of Figure 9, based on the amount of paint removed from the cable by wire breakage prior to the collapse, i.e., M2 had the most paint removed (the most wire breaks) while M3 had no paint removed (no wire breaks). Once M2 failed, the level of overload, plus the dynamic effects of the sudden failure of M2, were simply too great to be supported by the remaining cables. The collapse had been predicted by Thornton Tomasetti (2020), as cited previously. The service cable SC broke approximately 6 seconds after M3 as a result of the cables of Tower 12 impacting the catwalk bridge during the pendulum swing of the platform, thus overloading the service cables that supported it.

Estimates of the platform dynamics during the pendular swing

The system was modeled analytically as a pendulum (one degree of freedom) with the end of the pendulum string pinned to the middle point of an imaginary line between the tops of towers 8 and 12. The length of the pendulum string was calculated as $L = 357.5$ ft, using known dimensions from the observatory that were used by Morales (2006). It is also known that the lower corner of the platform (attachment points of main cables) was located 130.4 ft below the top of the towers, which sets the initial point for the pendulum swing. The point of interest in the calculations is at the bottom of the pendulum swing, i.e., the point at which the string becomes vertical. At this point, the speed and centripetal (normal) acceleration reach their maximum values.

The non-linear differential equation of motion of the pendulum can be easily derived in polar coordinates and is included as equation (15). It assumes that there is no air resistance, no friction at the pinned end, and all the mass is lumped at the free end. The Mathematica software was used to solve the equation with numerical integration. The elapsed time to the bottom of the swing was calculated by Mathematica as $t = 5.75$ seconds. The control video (NSF, 2020a) shows an elapsed time of approximately 6 seconds from the start of the pendular swing to the bottom of the swing (instant where the catwalk bridge is impacted and breaks). The comparable results (~ 5% error) show that the assumptions are reasonable to conduct additional estimates.

$$\frac{d^2\theta}{dt^2} + \frac{g}{L} sin\ sin\ (\theta) = 0 \tag{15}$$

Assuming that the potential energy due to the height of the platform was fully transformed to kinetic energy at the bottom of the swing (principle of conservation of energy), and using the above assumptions, the speed of the platform at the bottom of the swing was calculated at v = 120.9 ft/s = 82.4 mi/hr (equation (16)). Exactly the same results were obtained from the solution of the non-linear differential equation with Mathematica.

$$v = \sqrt{2gh} = \sqrt{2(32.2\ \frac{ft}{s^2})(357.5\ ft - 130.4\ ft)} = 120.9\ \frac{ft}{s} = 82.4\ \frac{mi}{hr} \tag{16}$$

Also, the speed formula based on conservation of energy may be combined with the definition of normal (centripetal) acceleration while assuming a radius of curvature "ρ" equal to the pendulum string length. The resulting normal acceleration at the bottom of the swing would have been 1.27 g's, where 1 g = 32.2 ft/s^2. (Equation (17)).

$$a_n = \frac{v^2}{\rho} = \frac{(\sqrt{2gh})^2}{L} = \frac{2g(357.5\ ft - 130.4\ ft)}{357.5\ ft} = 1.27g \tag{17}$$

Based on a free body diagram of the pendulum at the bottom of the swing, and ensuring dynamic equilibrium in the vertical direction, the vertical component of the total tension in the cables at the bottom of the swing would have been 2.27 times the platform weight (equation (18)).

$$T = W + ma_n = mg + m(1.27g) = 2.27mg = 2.27W \tag{18}$$

The combined factors of the increased tension in the cables due to the dynamic effect of the pendular motion, the more inclined angle of the cables at the bottom of the swing, the fact that the cables were now re-oriented between the strong axes of the towers of cruciform cross-sectional shape, the inefficiency of the backstays in this new orientation of the cables, and the rupture of the service cables (the only remaining elements connecting the three towers) ended up collapsing the top portions of towers 8 and 12 toward each other. In the case of tower 4, the top portion collapsed backward because the backstays pulled it back once the service cable snapped. Also, the sudden release of stored elastic energy in the service cable contributed to the backward collapse of tower 4. It is interesting that in the case of the shorter towers 4 and 12, only the top portion collapsed while in the case of the taller tower 8, the upper two portions collapsed.

Figure 10 shows the variation with time of the angle θ(t) obtained by solving the nonlinear equation of motion (15). The initial position is $\theta(0) = 68.6^o$. The green dot indicates the instant at which the pendulum passes through the vertical position.

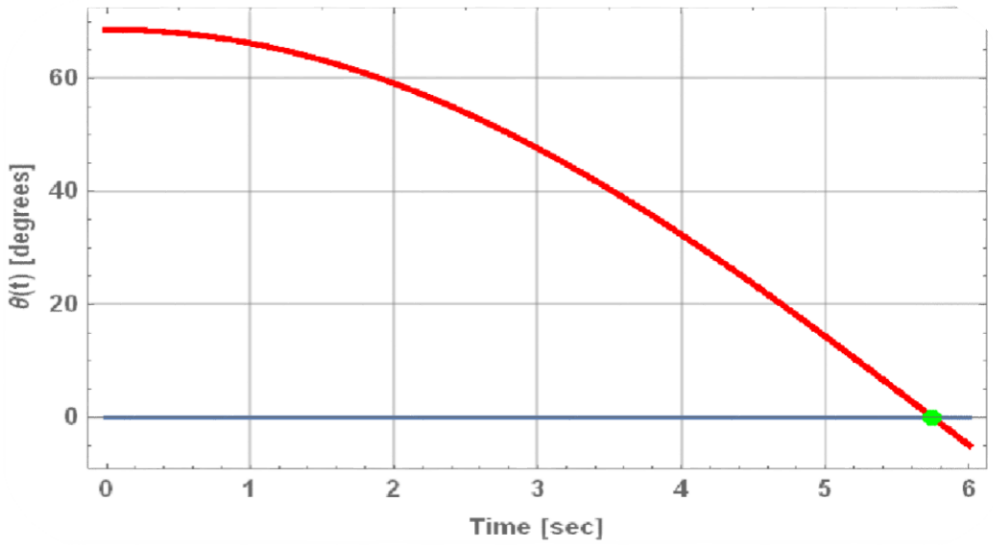

Figure 10: Time variation of the angle θ(t) of the pendulum.

Figure 11 displays the tangential velocity of the bob of the pendulum as a function of time. The green dot indicates the instant at which the pendulum passes through the vertical position and the velocity attains a maximum.

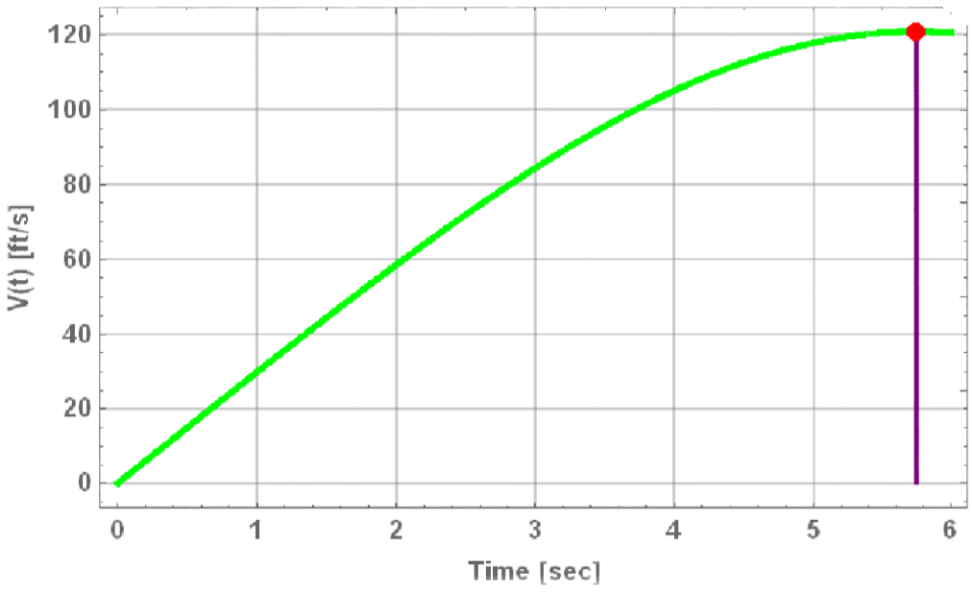

Figure 11: Time variation of the tangential velocity *V*(t) of the pendulum.

Accelerogram recorded during the event

Figure 12 shows an accelerogram (z-axis, vertical) during the final collapse. The accelerometer is located at the site of the observatory near tower 12. It was installed and operated by the Puerto Rico Seismic Network (PRSN) of the University of Puerto Rico at Mayagüez (UPRM) and had been operational for approximately 10 years. The signal was retrieved and processed by Dr. Elizabeth Vanacore, seismologist of the PRSN and associate professor at the Department of Geology of UPRM.

A time scale was included as an inset to compare times versus the video footage (NSF, 2020a). The table that is presented below the accelerogram synchronizes times with the control room footage, the drone footage, and the time scale in the accelerogram. Both footages are available in NSF (2020a). The footage times are precise to the nearest second and there are some apparent discrepancies with the accelerogram time scale (1 second discrepancies) which are highlighted in red in the last column. The origin of the time scale (t = 0 s) was placed at the highest acceleration peak which, after synchronizing the events, most likely represents the instant at which the platform impacted the hill. This seems reasonable because the platform was massive (about 700 tons after shedding the dome and the Azimuth arm) and moving at a speed close to 80 mi/hr., as calculated in the previous section. Notes were placed within the accelerogram to indicate the most likely events, based on the table. The impact of the Azimuth arm and the dome are not noted because this instant was not captured by the cameras. However, it is estimated that they impacted the dish at just about the same time that the towers failed (t = -2 sec).

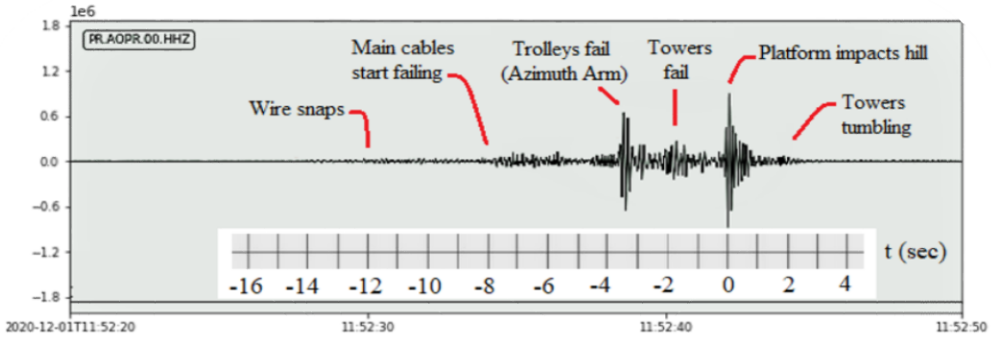

Event	Control Room footage time	Drone footage time	Accelerogram time scale
Wire snaps	N/A	1:01	-12
Main cables start failing	0:10	1:04	-8
Last main cable fails. Start of pendular swing.	0:11	1:05	-7
Trolleys of Azimuth Arm start failing	0:14	N/A	-5
Azimuth Arm and Dome break off	0:16	N/A	-3
Towers fail at the bottom of the swing (catwalk bridge breaks)	0:17	1:11	-2
Platform impacts the hill	0:19	1:13	0
Tumbling tower 12	0:22	1:16	+2
Tumbling tower 8	N/A	1:16	+2

Figure 12: Accelerogram obtained during the collapse event. Provided by Elizabeth Vanacore of PRSN. The Control Room and Drone footage times were taken from the NSF video (NSF, 2020a).

CONCLUSIONS

Despite the limitations of time and available information, the following is concluded:

1. Corrosion does not seem to have played a significant role in any of the three events discussed in this article.

2. The slippage of the auxiliary cable from its socket termination (first cable failure) was most probably caused by manufacturing flaws during the fabrication of the cable/socket connection.

These will be reviewed and updated once the forensic analyses are concluded and made public.

ACKNOWLEDGMENTS

The authors gratefully acknowledge the staff of the journal for their assistance in the preparation of this manuscript. We would also like to thank Dr. Elizabeth A. Vanacore, of the PRSN and Department of Geology of UPRM, and Dr. José A. Martínez Cruzado, of the Puerto Rico Strong Motion Program and Department of Civil Engineering of UPRM, for providing the accelerogram recorded during the collapse and for providing initial clues on its interpretation.

REFERENCES

Bradon, J. E., and Ridge, I. L. (2003). "Comparison of white metal and resin socket terminations for wire ropes", *The Journal of Strain Analysis for Engineering Design*, Vol. 38, No. 2, pp. 149-160.

Certex (2020). "Wire rope terminations", Certex USA, Charlotte, North Carolina, https://www.google.com/url?sa=t&rct=j&q=&esrc=s&source=web&cd=&cad=rja&uact=8&ved=2ahUKEwiI-MrmjO7tAhVOrFkKHTjCAsQQFjAAegQIARAC&url=https%3A%2F%2Fcertex.com%2Fwp-content%2Fuploads%2Fwire-rope-terminations.pdf&usg=AOvVaw0fUYtnvOReQB5PWWateMLr

Chavel, B.W. and Leshko, B.J. (2012). "Primer for the Inspection and Strength Evaluation of Suspension Bridge Cables", Report FHWA-IF-11-045, HDR Engineering Inc., Pittsburgh, Pennsylvania.

Coto, D. (2020). "Cable failures endanger renowned Puerto Rico radio telescope", Associated Press, November 15. https://apnews.com/article/technology-arecibo-observatory-science--053fbf8834e50d5e3ad88443a3fde550

DIN 3092-1 (1985). "Socketing of Wire Ropes - Casting in Metal - Safety Requirements and Testing", Deutsches Institut fur Normung E.V. (DIN), Germany.

Drake, N. (2020). "Iconic radio telescope suffers catastrophic collapse", National Geographic, December 1. https://www.nationalgeographic.com/science/2020/12/arecibo-radio-telescope-in-puerto-rico-collapses/

Metcalf Jr, J. T., and Matanzo Jr, F. T. (1980). "Wire rope terminations, section, and replacement criteria", Offshore Technology Conference, Houston, Texas. May 5-8.

Morales, J. C. (2006). "Dynamic properties and seismic response of the cable structures and towers of the Arecibo Observatory", PhD dissertation, Department of Civil Engineering and Surveying, University of Puerto Rico at Mayagüez, Puerto Rico.

NAIC (2020a). "Astronomy", Arecibo Observatory. https://www.naic.edu/ao/astronomy

NAIC (2020b). "Telescope Description", Arecibo Observatory. https://www.naic.edu/ao/telescope-description

NAIC (2020c). "Arecibo Observatory Construction", Arecibo Observatory. http://www.naic.edu/history_gal/historicgal.html

NAIC (2020d). "Broken cable damages Arecibo Observatory", Arecibo Observatory, August 11. https://www.naic.edu/ao/node/1169

NAIC (2020e). "A second cable fails at NSF's Arecibo Observatory in Puerto Rico" Arecibo Observatory, November 8. https://www.ucf.edu/news/a-second-cable-fails-at-nsfs-arecibo-observatory-in-puerto-rico/

NAIC (2020f). "Arecibo Observatory Telescope to be Decommissioned After Second Cable Break" Arecibo Observatory, November 19. https://www.ucf.edu/news/arecibo-observatory-telescope-to-be-decommissioned-after-second-cable-break/

National Academies (2005). "Inspection and Maintenance of Bridge Stay Cable Systems", The National Academies Press, Washington, DC: https://doi.org/10.17226/13689

NSF (2020a). "Footage of Arecibo Observatory telescope collapse", National Science Foundation, December 3. https://www.youtube.com/watch?v=ssHkMWcGat4

NSF (2020b). "Media briefing: Arecibo Observatory 305-meter telescope update", National Science Foundation, December 3. https://www.nsf.gov/news/special_reports/arecibo/2020_12_03_AreciboBriefing_Transcript_FINAL.pdf

RR-S-550 Rev. D (1980). "Federal Specification Sockets, Wire Rope", U.S. General Services Administration – Federal Acquisition Service, Washington, D.C.

RR-S-550 Rev. F (2018). "Federal Specification Sockets, Wire Rope", U.S. General Services Administration – Federal Acquisition Service, Washington, D.C.

Thornton Tomasetti (2020). "Recommendation for Course of Action at Arecibo Observatory", Memorandum to Ramón Lugo dated November 12, Thornton Tomasetti, Inc., New York, New York

Tokyo (2020). "Wire Rope Catalog", Volume 5. Tokyo Rope Manufacturing Co., LTD, Tokyo, Japan.

Verreet, R. (1997). "Wire rope end connections", Casar Wire Ropes, Casar Drahtseilwerk SAAR GMBH, Kirkel, Germany.

Wall, M. (2020). "Arecibo Observatory in Puerto Rico suffers serious damage after cable breaks", Space.com, August 13. https://www.space.com/arecibo-observatory-damaged-shut-down.html

Wirelock (2017). "Technical Data Manual", version 2-11/17, Millfield Enterprises (Manufacturing) Limited, Newcastle upon Tyne, United Kingdom.

WJE (2020). "Arecibo Observatory Stabilization Efforts", Memorandum WJE No. 2020.5191 to Ramón Lugo, dated November 12, Wiss, Janney, Elstner Associates, Inc., Indianapolis, Indiana.

WSP (2020). "Recommendations for future efforts at Arecibo Observatory", Memorandum to Ramón Lugo, dated November 11, WSP USA Solutions, Inc., New York, New York.